WINTER STORM STUDIES: COMPARISON OF OBSERVATIONS FROM A 2-D VIDEO DISDROMETER AND POLARIMETRIC RADAR

Report Prepared for the Federal Aviation Administration

30 September 2004

Kyoko Ikeda, Edward A. Brandes, and Guifu Zhang

National Center for Atmospheric Research
P.O. Box 3000
Boulder, Colorado 80307

1. Introduction

The Winter Icing and Storms Project 2004 (WISP04) was conducted from February to April 2004 in north central Colorado. Program objectives were to evaluate remote sensing techniques for icing detection and to quantify winter precipitation in support of airport deicing operations. Measurements from a S-band dual-polarization radar and a two-dimensional video disdrometer are being used to develop radar-based algorithms to discriminate between rain and snow, quantify winter precipitation, and improve parameterization of winter precipitation in numerical forecast models. Winter precipitation often includes periods with liquid, mixed-phase, and frozen hydrometeors. An ability to match radar-measured and disdrometer-based radar parameters is essential when developing radar-based algorithms for winter precipitation. Disdrometers provide important information regarding hydrometeor size, terminal velocity, shape, and number concentration at high temporal resolution. As a first step, we verify that the radar detects subtle changes in the character of winter precipitation.

Here radar reflectivity factor (reflectivity or Z_H, hereafter) and differential reflectivity (Z_{DR}) are calculated from disdrometer data collected on 5 March and 20 February 2004, events in which precipitation changed from rain to snow. The calculations are based on scattering amplitudes of raindrops and snowflakes computed with the T-matrix method. Particle bulk density during transition and snow phases was allowed to vary according to an empirical relation between particle size and bulk snow density developed with disdrometer observations. Reflectivity and differential reflectivity calculations based on disdrometer observations show good agreement with radar measurements.

The dataset and a brief description of the disdrometer are given in section 2. Section 3 discusses the retrieval method for reflectivity and differential reflectivity followed by a comparison with radar measurements (Sections 4 and 5). A summary with concluding remarks is given in section 6.

2. Data

The radar data were collected with NCAR's S-band dual-polarization radar located at Marshall, Colorado. Scan strategies included sector scans at 0.5 and 1.5^o elevation and range-height indicator (RHI) scans over a 2-D video disdrometer placed at a range of 19 km and an azimuth angle of 42° from the radar.

The disdrometer consists of two line-scan cameras providing front and side views of hydrometers falling into the instrument. Each camera has a single line of 700 photo-detectors positioned opposite a light source. Hydrometeors falling through the 10 cm by 10 cm measuring area block the light source, shadowing some photo-detectors at a resolution of 0.15 mm. The number of blocked photo-detectors is recorded for each camera at a frequency of 34.1 kHz. The vertical resolution, which depends on the terminal velocity of the particle, is generally 0.1 mm for rain and 0.03 mm for snow falling at 1 m s^{-1}. The sampling creates image projection slices of the hydrometeors.

Information provided on individual hydrometeors includes silhouette images, height and width information from each camera, and the particle terminal velocity. Particle terminal velocity is computed from the vertical distance between the two camera planes and the time the hydrometeor takes to break each plane. Raindrop axis ratio, canting angle, and horizontal velocity are also obtained. The disdrometer is equipped with temperature and wind sensors. A detailed description is found in Kruger and Krajewski (2002). Field notes from a crystal observer supplement the disdrometer data for the 5 March 2004 case. Observations of crystal type, size, degree of riming, and amount of aggregation were made every 15 minutes.

3. Modeling considerations

Radar reflectivity (in mm^6 m^{-3}) at horizontal (H) and vertical (V) polarization can be computed from

$$Z_{H,V} = \frac{4\lambda^4}{\pi^4 \left|K_w\right|^2} \sum_{i=1}^{M} N(D_i) \left| f_{H,V} \right|^2 \Delta D \qquad (1)$$

where λ is the radar wavelength, K_w is the dielectric factor of water, $N(D_i)$ is the number concentration for the *i*th size category having an equivalent diameter (mm) between D_i and $D_i + \Delta D$, M is the total number of size categories, and $\left| f_{H,V} \right|$ is the scattering amplitude at horizontal and vertical polarization (see Zhang et al. 2001). In this study, the disdrometer data were quantitized into size categories of 0.2 mm over the range of 0.1-20.1 mm for snow and 0.1-8.1 mm for rain. Reflectivity is expressed in dBZ ($10\times\log_{10}Z_H$).

The differential reflectivity (Z_{DR} in dB) is defined as

$$Z_{DR} = 10\times\log_{10}(Z_H / Z_V)\,. \qquad (2)$$

Z_{DR} is sensitive to particle bulk density and canting angle and can be interpreted as the reflectivity-weighted mean axis ratio of the illuminated hydrometeors. The Z_{DR} values were corrected for system bias (–0.08 dB). The bias was determined from radar data obtained by pointing the antenna vertically in light rain. In theory, raindrops should produce a Z_{DR} of 0 dB in the mean when viewed from below.

Scattering amplitudes were computed with the T-matrix method (Barber and Yeh 1975). Input parameters include the dielectric constant, particle shape (e.g., axis ratio), and temperature. For rain these parameters follow Zhang et al. (2001).

Properties of snow are complex. Aspect ratios and bulk densities continuously change throughout storm evolution making computations of the scattering amplitudes less straight

forward than for rain. In this study, the particles were assumed to be oblate spheroids having a fixed axis ratio (vertical divided by horizontal) of 0.7.

The effective dielectric constant (Ishimaru 1991) was derived using disdrometer data collected at Marshall prior to the WISP04 field program. Snow bulk density was computed from disdrometer measurements of precipitation volume and mass measurements from gauges. All instruments were located inside wind shields. The relation between the median equivolumetric diameter (D_0) and bulk density for 16 time segments that were selected from nine snow events with ambient winds less than 2 m s^{-1} is shown in Fig. 1. The time segments ranged between 30 minutes and 2 hours in duration and were chosen based on the steadiness of particle concentrations and similarities in hydrometeor characteristics. Data points are from particle size distributions (PSD) averaged over 5 minutes (dots) and over each time segment (asterisks). Power-law relations fitted to the 5-minute and the segment PSDs are overlaid. The dataset contains both rimed and unrimed snow. Nevertheless, the data generally follow the inverse relation between size and density found by Holroyd (1971) for unrimed snowflakes. For this study, we use an effective dielectric constant based on the power-law relation corresponding to the 5-minute PSDs. In a sense, the computed scattering amplitude allows for a variation in bulk density that is anticipated to occur with storm evolution. This approach is similar to that taken by Ryzhkov et al. (1998) who proposed a method to compute cloud ice water content using a relation between particle bulk density and radar cross sections.

4. Observations: 5 March 2004

Precipitation on 5 March 2004 was dominated by an intense 500 mb trough across the western United States and an associated surface low pressure system over central Oklahoma. Low-level winds from the east-northeast and northeast behind the low pressure center created a favorable condition for a upslope stratiform precipitation in the WIPS04 domain. Winds above 3 km MSL, i.e., above the upslope layer, were mostly westerly or southwesterly. An abrupt decrease in temperature from 5.5^{o}C to 0.5^{o}C occurred over a 15-minute period at approximately 0100 UTC. The surface temperature changed only slightly afterward remaining between 0.5 and –0.5^{o}C. The temperature at cloud top (5 km MSL) was –15°C.

a. Precipitation

Most of the precipitation fell between 0000 and 0500 UTC. Table 1 summarizes the hydrometeor types noted by the crystal observer. Early precipitation was light rain (Period A). The surface layer moistened and cooled rapidly as the rain rate increased. A rain-to-snow transition (Period B) occurred with the temperature decrease at 0100 UTC. Field notes indicate ice pellets were mixed with raindrops (Fig. 2). The smaller terminal velocities of ice pellets, compared with raindrops, are evident in the disdrometer data (Fig. 3, Period B). [Terminal velocity relations for raindrops, graupel and aggregates are plotted as a reference.] A small number of large aggregates also existed at this time which caused an increase in the particle median volume diameter (Fig. 4). Mixed-phase precipitation ended by 0120 UTC.

Later (0120-0145 UTC; Period C), observed precipitation consisted mostly of ice pellets and some small aggregates. Beginning at 0145 UTC (Period D), 1-3 mm plate-like crystals (plates and dendrites) became noticeable, and the number of large aggregates increased significantly. (Figs. 2 and 3, Period D). The observed terminal velocities show a weak

Table 1: Summary of observations taken at the disdrometer site. Hydrometeors are listed from most to least dominant. Typical aggregate sizes (mm), percentage of total particles identified as aggregates, and degree of riming (none, light, moderate, heavy) are noted.

	Time (UTC)	Hydrometeors	Aggregates	Temperature (^{o}C)
A	0000-0100	Rain	—	5.5-7
B	0100-0120	Rain mixed with ice pellets	none	0.5-5.5
C	0120-0145	ice pellets	3-8 mm 30 % light	0.5
D	0145-0220	dendrites, plates, stellars	3-10 mm 40 % light to mod.	0.1
E	0220-0400	irregular snow, lump graupel	2-5 mm 5-20 % light	–0.5-0.1

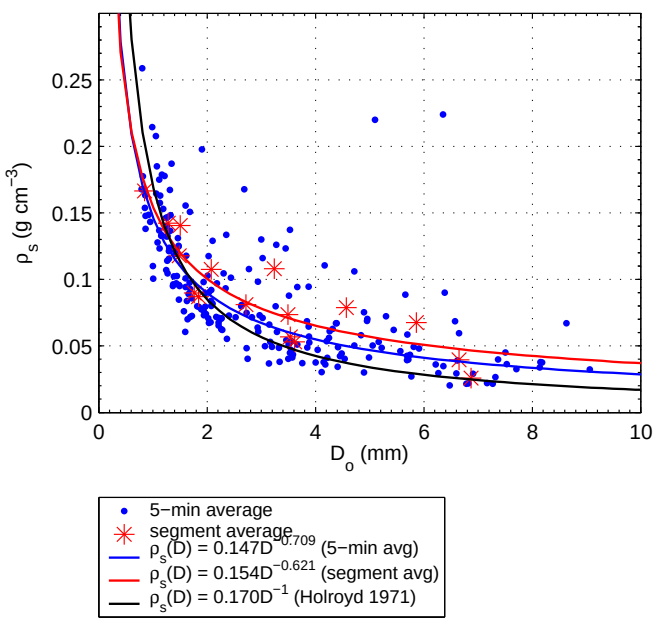

Figure 1:Relation between snow bulk density (ρ_s) and median volume diameter (D_o) for selected snow events between February 2002 and February 2004. Dots are for PSDs averaged over 5 minutes. Asterisks represent averaged values over selected longer time segments of the snow events. The blue (red) line is a power-law relation derived from the 5-minute (segment) averages. The black line is a relationship for unrimed snow aggregates from Holroyd (1971).

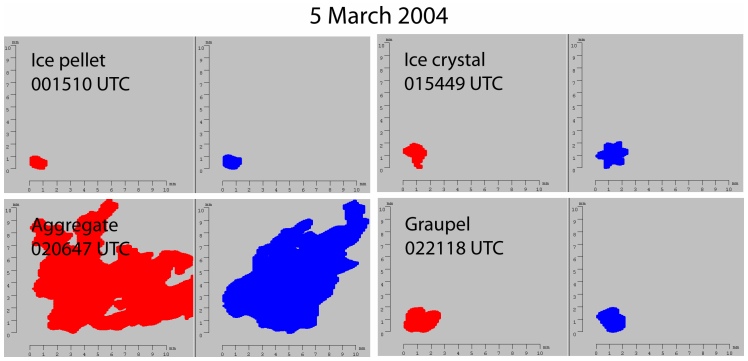

Figure 2: Sample hydrometeor images from Period B (ice pellet), Period D (ice crystal and aggregate), and Period D (graupel) . Red and blue images are the front and side views, respectively. The width and height scales are in mm.

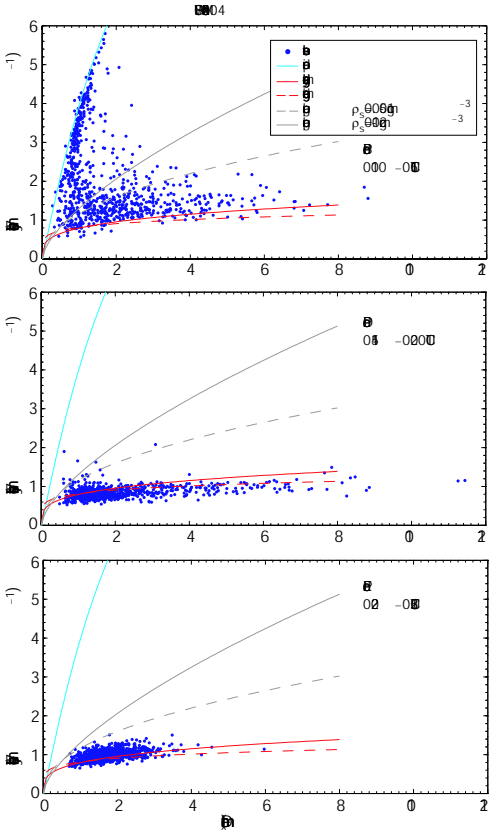

Figure 3: Particle terminal velocity versus diameter for time segments in Period B (top), Period D (middle), and Period E (bottom). Hydrometeor observations during these time periods are indicated in Table 1. Data points represent 1-second volume-weighted terminal velocities at sea level. The terminal velocity relation for rain is from Brandes et al. (2002). Relations for graupel and snow aggregates are from Locatelli and Hobbs (1974).

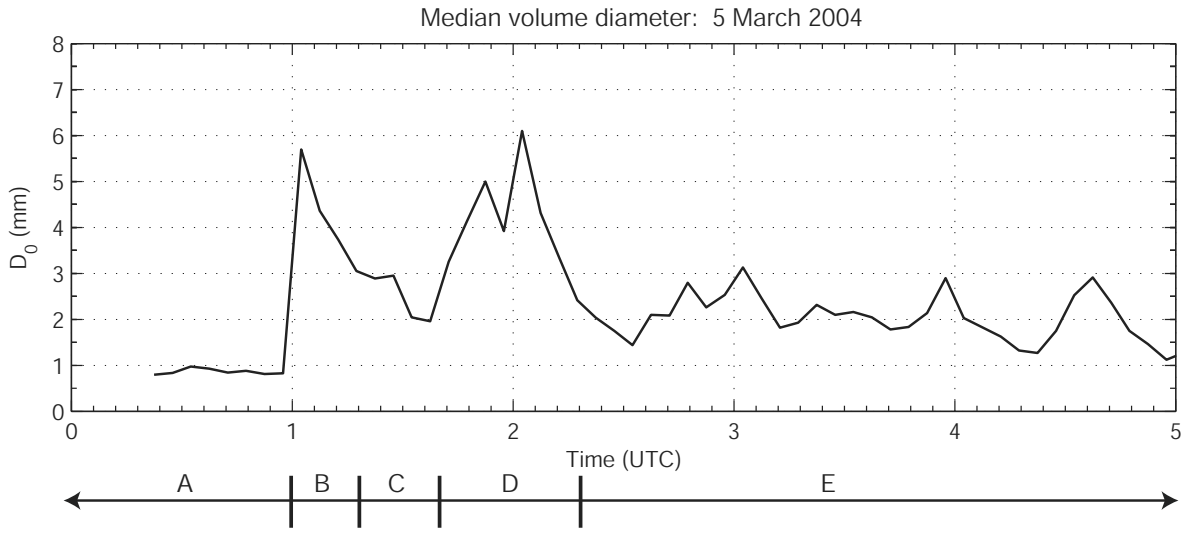

Figure 4: Time history of median equivolumetric diameters (D_0) from 5-minute PSDs.

relationship with aggregate size and follow the unrimed aggregate relation from Locatelli and Hobbs (1974).

At ~0220 UTC, another change in particle habit occurred (Period E). Hydrometeors were identified as small lump graupel and irregular snow pellets (Figs. 2 and 4). Field notes indicate much less aggregation at this time. The terminal velocity appears to have a slightly stronger size-dependency compared with the previous period (Fig. 3, Period E). The median volume diameter decreased significantly between heavy aggregation during Period D (D_0 = 6 mm) and the subsequent graupel/snow pellet Period E ($D_0 \leq$ 3 mm). This change suggests an increase in bulk density for the latter period (Fig. 1).

b. Comparison of the measured and calculated Z_H and Z_{DR}

Figure 5 shows time histories of measured and derived Z_H and Z_{DR}. The derived Z_{DR} values were computed with an assumed Gaussian canting angle distribution having a mean of 0° and standard deviations (σ_ϕ) of 0, 20, and 30°. The radar measurements are averaged over 1 km in the horizontal at the disdrometer site. [The 0.5 and 1.5^o elevation radar beams were about 400 and 750 m above the disdrometer.] Cross sections of Z_H and Z_{DR} were uniform in the horizontal; thus, the computations do not take particle trajectories into account.

The Z_H retrievals with the disdrometer data in Period A are slightly less than the radar measurements. The Z_H cross sections in the early rain stage show an elevated layer of maximum reflectivity at ~3 km. Evaporation at low levels may account for the offset between the estimated and measured values. If Z_H is computed assuming that the particles during the rain period (Period A) are snow, the retrievals are significantly less than the measurements, reflecting the dependency of Z_H on the hydrometeor dielectric constant.

Agreement between the measured and derived Z_H are excellent during the snow period (after 0100 UTC). Well-matched retrievals in Period B, when using the snow scattering amplitude, probably come from the fact that radar return signals from large, low density

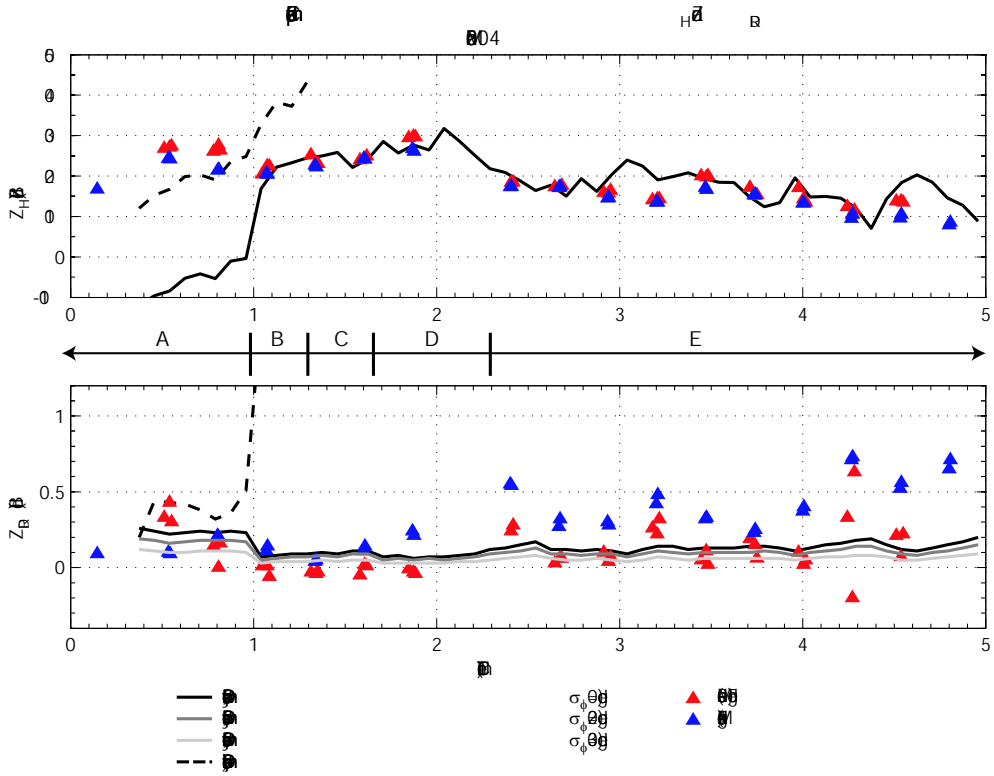

Figure 5: Time histories of measured and retrieved Z_H (top) and Z_{DR} (bottom). Retrievals (solid and dashed lines) are based on 5-minute PSDs. Dark, intermediate, and light solid lines are for retrievals with canting angle (σ_ϕ) of 0, 20, and 30 degrees, respectively. Radar measurements (triangles) are averaged over 1 km in the horizontal.

aggregates dominated the returns from the smaller raindrops and ice pellets. An overall reduction in particle size and an associated decrease in snowfall rate (Period D and Period E) cause a Z_H reduction of about 10 dBZ.

Similarly, Z_{DR} calculations and measurements for the respective rain and snow phases show good agreement. As with reflectivity, Z_{DR} retrievals based on raindrop scattering amplitudes greatly exceed the measurements during the rain-snow transition period. Correspondence for the snow period is attributable in large part to accounting for particle density changes. Small Z_{DR} is associated with low density aggregates in Period B through Period D. The measured and retrieved Z_{DR} values slightly increased when the number of aggregates significantly decreased and small graupel and snow pellets with higher density became dominant (Period E). This Z_{DR} increase did not occur if the bulk density was fixed at a constant value (not shown). During Period E, the measured Z_{DR} decreases toward ground (compare values at 0.5 and 1.5^o elevation). This suggests that particles were more pristine at higher elevations during

this stage and that riming and/or aggregation was taking place between the two scan levels causing the particles to become less oblate in the mean as they fell.

Ice particles may have significant canting angles depending on their particular habits. Aggregates may flutter while falling (e.g., Kajikawa 1982). Graupel, dominant in Period E, tends to tumble (Zimunda and Vali 1972). However, the sensitivity of Z_{DR} computations to assumed particle canting angles appears to be small (Fig. 5, lower panel). The spread between the three snow-density based curves is minimal in Periods B through D and increases only when graupel becomes dominant. Also, canting angles are not important for low density particles.

5. Observations: 20 February 2004

A short precipitation event occurred between 0000 and 0200 UTC on 20 February 2004. Synoptic conditions were similar to that on 5 March 2004. On this day a strong northerly barrier jet (Marwitz and Toth 1993) developed after 0000 UTC. As the jet intensified, temperature at the disdrometer site decreased from 2 to 0.5°C. Z_H cross sections showed pronounced vertical structures with precipitation fallstreaks extending downward from near cloud top where the northerly low-level winds gave way to westerly upper-level winds (Fig. 6). Because there was significant vertical structure, comparisons of the derived and measured Z_H and Z_{DR} account for particle trajectories.

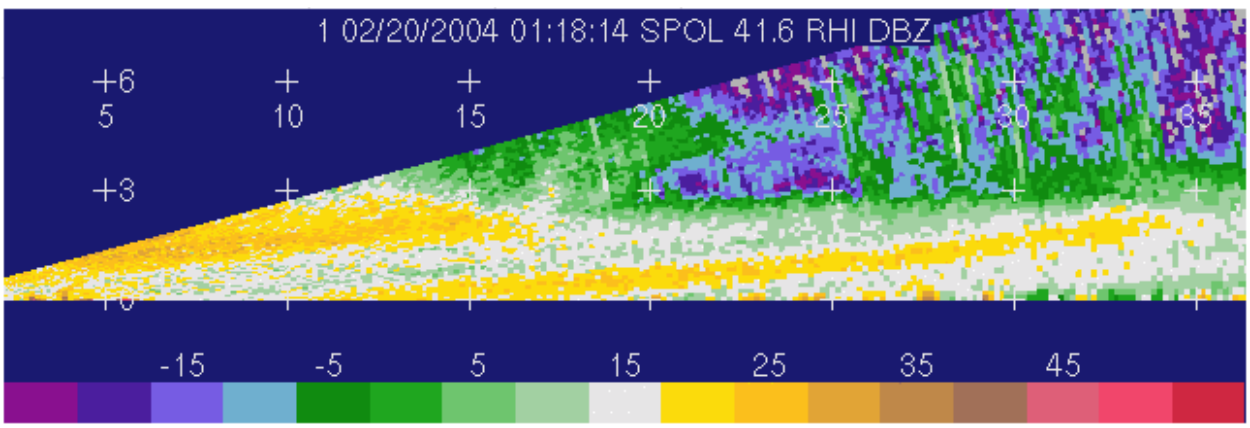

Figure 6: A cross section of radar reflectivity at 41.6° azimuth for 0118 UTC on 20 February 2004. The pluses indicate 5-km intervals in the horizontal and 3-km intervals in the vertical (above ground level). The disdrometer site is at a range of 19 km.

a. Precipitation

Corroborating in situ observations of hydrometeors are not available for this case. Instead, changes in hydrometeor types were inferred from the disdrometer data. Light rain began just before 0000 UTC (Period A). A period of rain mixed with snowflakes (Period B) began at 0030 UTC, and moderately-sized aggregates dominated between 0100 and 0115 UTC (Period

C). Particle images and terminal velocities indicate that precipitation was essentially rain after 0120 UTC (Period D).

b. Comparison of the measured and calculated radar parameters

Similar to the previous case, the PSD-based estimates of Z_H and Z_{DR} agree with radar measurements (Fig. 7). The correspondence of the Z_H retrieval assuming the density for rain during Periods A and D is good. Period B, consisting of mixed-phased hydrometeors, shows better agreement when using raindrop scattering amplitudes. This result differs from the rain-snow transition on 5 March 2004 (section 4, Period B) in which the snow-density based Z_H retrieval produced better correspondence with the radar measurements. The difference appears related to the dominant precipitation type. Mixed-phase precipitation on 20 February 2004 was composed mostly of raindrops (resulting in a higher value of effective dielectric constant), while on 5 March 2004 aggregates clearly dominated (Fig. 3, Period B).

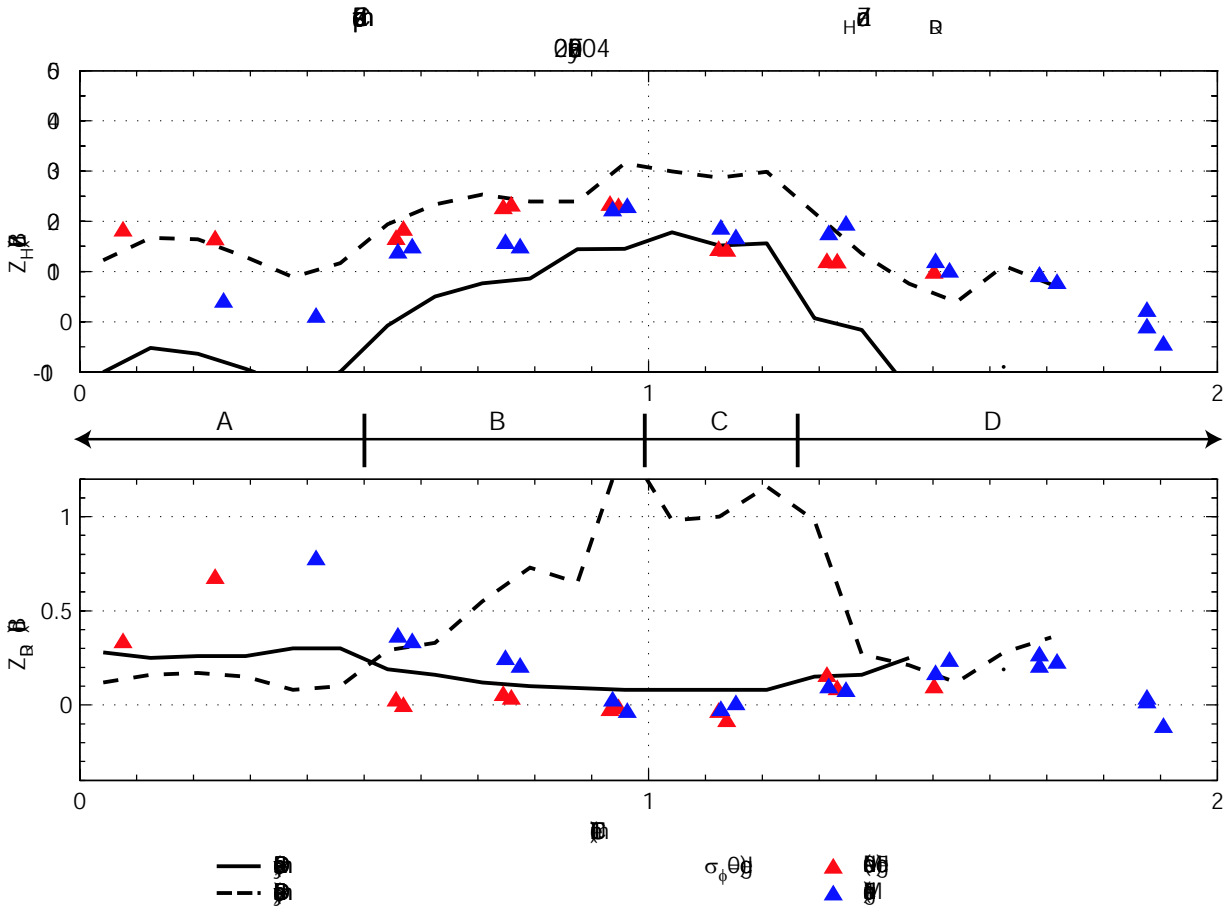

Figure 7: Same as Fig. 5 but for 20 February 2004. The snow-density based retrievals for only σ_ϕ=0° is shown. Precipitation characteristics for Periods A-D are described in the text.

Measurements from only one radar volume scan are available during the snow period (Period C). Nevertheless, the computed Z_H based on the snow-density relation matches the measurements. During Periods B and C, the retrieved Z_{DR}s also agree with the measurements. The overestimates of Z_{DR} when raindrops are assumed is explained by large D_0 (2 to 6 mm) derived from the PSDs (not shown). Again, more realistic Z_{DR} values were achieved using the relationship between the snow bulk density and characteristic size (D_0).

6. Summary and concluding remarks

Radar reflectivity and differential reflectivity were computed from disdrometer data and compared to radar measurements from WISP04 events of 5 March and 20 February 2004. Scattering amplitudes for snow particles were derived by exploiting an empirical relationship between particle size and snow bulk density. Overall, the comparisons showed good agreement. Large positive biases in the Z_H and Z_{DR} retrievals during the snowflake-dominated mixed-phase period on 5 March when applying the scattering amplitudes for raindrops disclose the importance of knowing the correct dominant hydrometeor type. The correspondence between the Z_H measurements and the raindrop-based retrievals of Z_H during the rain-dominated mixed-phase period on 20 February further confirms the need to identify the dominant hydrometeor type.

Radar measurements and disdrometer calculations for the snow period on 5 March agreed nicely. Aggregates were associated with small Z_{DR} and large Z_H, as expected. An increase in bulk density, as the number of aggregates decreased and that of compact graupel increased, was reflected by a general increase in Z_{DR} and decrease in Z_H. In this case, the use of the size-density relation was important in achieving good agreement between the retrievals and measurements.

A sensitivity study reveals that particle canting angles have little impact on disdrometer calculations of Z_{DR} for low density snow particles. Further studies are necessary to assess the importance of canting angles for higher density particles such as graupel and pristine ice crystals. Future studies will also explore the importance of particle axis ratios.

Reproduction of radar parameters with disdrometer observations is an important initial step in the development of radar-based algorithms for characterizing winter precipitation. Well-matched retrievals provide a foundation for reconstructing particle size distributions. Such a capability is required for improving microphysical parameterizations in numerical forecast models and for quantifying winter precipitation from polarimetric radar measurements.

References

Barber, P., and C. Yeh, 1975: Scattering of electromagnetic waves by arbitrarily shaped dielectric bodies. *App. Optics*, **14**, 2864-2872.

Brandes, E. A., G. Zhang, and J. Vivekanandan, 2002: Experiments in rainfall estimation with a polarimetric radar in a subtropical environment. *J. Appl. Meteor.*, **41**, 674-685.

Holroyd, E. W., III, 1971: The meso- and microscale structure of Great Lakes snowstorm bands: A synthesis of ground measurements, radar data, and satellite observations. Ph.D. dissertation, State University of New York at Albany, 148 pp.

Ishimaru, A., 1991: *Electromagnetic Wave Propagation, Radiation, and Scattering*. Prentice Hall, 637 pp.

Kajikawa, M., 1982: Observation of the falling motion of early snow flakes. Part I: Relationship between the free-fall pattern and the number and shape of component snow crystals. *J. Meteor. Soc. Japan*, **60**, 797-803.

Kruger, A., and W. F. Krajewski, 2002: Two-dimensional video disdrometer: A description. *J. Atmos. Oceanic Technol.*, **19**, 602-616.

Locatelli, J. D., and P. V. Hobbs, 1974: Fall speeds and masses of solid precipitation particles. *J. Geopys. Res.*, **79**, 2185-2197.

Marwitz, J., and J. Toth, 1993: The front range blizzard of 1990. Part I: Synoptic and mesoscale structure. *Mon. Wea. Rev.*, **121**, 402-415.

Ryzhkov, A. V., D. S. Zrnic, and B. A. Gordon, 1998: Polarimetric method for ice water content determination. *J. Appl. Meteor.*, **37**, 125-134.

Zikmunda, J., and G. Vali, 1972: Fall patterns and fall velocities of rimed ice crystals. *J. Atmos. Sci.*, **29**, 1334-1347.

Zhang, G., J. Vivekanandan, and E. Brandes, 2001: A method for estimating rain rate and drop size distribution from polarimetric radar measurements. *IEEE Trans. Geosci. Remote Sens.*, **39**, 830-841.